AD-A194 591 CORONAL MAGNETIC FIELDS PRODUCED BY PHOTOSPHERIC SHEAR (U) STANFORD UNIV CA CENTER FOR SPACE SCIENCE AND ASTROPHYSICS J A KLIMCHUK ET AL APR 88 1/1

UNCLASSIFIED CSSA-ASTRO-87-17 N00014-85-K-0111 F/G 3/2 NL

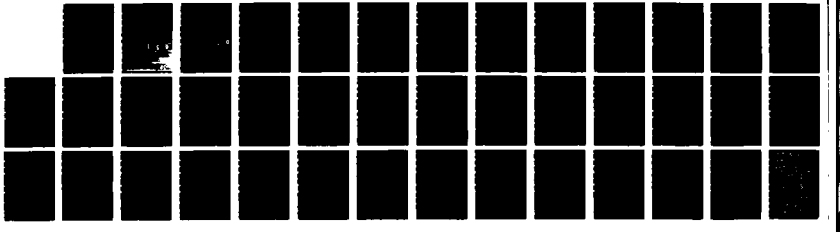

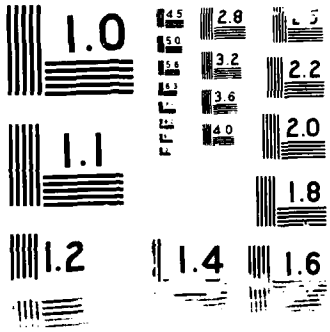
1.0
1.1
1.2
2.8
3.2
3.6
4.0
2.2
2.0
1.8
1.4
1.6

C S S A

CORONAL MAGNETIC FIELDS PRODUCED BY PHOTOSPHERIC SHEAR

Contract N00014-85-K-0111

J. A. Klimchuk and P. A. Sturrock

Center for Space Science and Astrophysics
Stanford University

W.-H. Yang

Center for Atmospheric and Space Sciences
Utah State University

CENTER FOR SPACE SCIENCE AND ASTROPHYSICS
STANFORD UNIVERSITY
Stanford, California

(4)

CORONAL MAGNETIC FIELDS PRODUCED BY PHOTOSPHERIC SHEAR

Contract N00014-85-K-0111

J. A. Klimchuk and P. A. Sturrock

Center for Space Science and Astrophysics
Stanford University

W.-H. Yang

Center for Atmospheric and Space Sciences
Utah State University

CSSA-ASTRO-87-17
April 1988

ABSTRACT

We use the magneto-frictional method for computing force-free fields to examine the evolution of the magnetic field of a line dipole, when there is relative shearing motion between the two polarities. We find that the energy of the sheared field can be arbitrarily large compared with the potential field. We also find that it is possible to fit the magnetic energy, as a function of shear amplitude, by a simple functional form. The fit parameters depend only on the distribution of normal field in the photosphere and the form of the shearing displacement. They show that the energy is relatively more enhanced if the shear occurs: (1) where the normal field is strongest; (2) in the inner region of the dipole, near the axis; or (3) over a large fraction of the dipole area.

I. INTRODUCTION

Stressed coronal magnetic fields play a key role in solar activity, providing the energy for solar flares and possibly for related activity such as surges and coronal mass ejections. (See, for instance, Priest 1982.) By "stressed," we mean that the coronal magnetic field is not current-free so that it is in a higher energy state than the corresponding magnetic field with the same normal magnetic field at the photosphere but without coronal currents. It is therefore important to try to understand the way in which such stressed magnetic-field configurations can develop and to estimate the "free energy" in such configurations. The "free energy" is the excess of the magnetic-field

energy of the current-carrying field above that of the corresponding current-free field.

There are several ways in which currents can develop in coronal magnetic-field configurations. One possibility is that a twisted flux tube emerges from below the photosphere. Another possibility is that two or more distinct flux systems are adjacent to each other, so that current sheets develop at the boundaries. The third possibility is that a field initially in a current-free state is stressed by photospheric motion. This is the possibility that we consider in this article.

Unfortunately, we do not yet have systematic data concerning the horizontal velocity fields in the photosphere of solar active regions. The new development of "correlation tracking," that has been demonstrated on a short span of data acquired during the *Spacelab II* mission (Simon *et al.* 1988), holds out the promise that such data can be acquired by spacecraft in the future. Such data would be most valuable in furthering our understanding of solar activity.

Nevertheless, there is circumstantial information indicating that horizontal velocity fields do play a significant role in stressing coronal magnetic fields. For instance, the occurrence of homologous sequences of flares indicates that, once a flare has occurred and returned the magnetic field to something approximating a current-free state, the field is again stressed so that another flare can occur, and so on. (See, for instance, Svestka 1976.) The similarity of flares in such sequences argues against attributing the re-stressing of the field to the eruption of new magnetic flux. It seems more likely that the progressive re-stressing is to be attributed to a steady photospheric horizontal velocity field.

Evidence that the magnetic fields of active regions are stressed, whatever the reason, comes in several different forms. Photospheric vector magnetograms often indicate a high degree of shear in the vicinity of magnetic neutral lines (e.g., Hagyard 1985). Indirect evidence of this shear at slightly higher altitudes is provided by dark structures observed in Hα , such as active region filaments, which are known to be associated with large "two-ribbon" flares (e.g., Athay et al. 1986; Klimchuk 1987). One interpretation of the *UVSP* C IV Dopplergram data from the *Solar Maximum Mission* spacecraft leads to the conclusion that shear may be present in the transition region (Athay et al. 1986). And finally, soft X-ray loops, such as those observed by *Skylab*, are suggestive of shear in the corona (e.g., Webb and Zirin 1980).

For these reasons, we are particularly interested in the coronal magnetic-field configurations that develop above photospheric regions containing a linear magnetic dipole, when there is a shear-like displacement on opposite sides of the dipole. In examining this problem, we assume that the density and pressure of the coronal gas are sufficiently small that the magnetic field is unaffected by gravitational and pressure forces. However, the electrical conductivity of the coronal gas will still be sufficiently high that the magnetic field is "frozen" into the coronal plasma. In such situations, the magnetic field will be force-free, and we are therefore faced with the problem of calculating force-free magnetic-field configurations (Priest 1982).

A procedure for calculating such configurations was developed some time ago by Sturrock and Woodbury (1967), and one example of a line dipole configuration was calculated at that time. We present in this

article a series of calculations which we have make using an improved computational procedure.

The quantity of greatest interest is the total magnetic energy in such a sheared magnetic-field configuration. This will of course be a function of the magnitude of the shear. We find that the results of our detailed calculations may be fit by a simple formula that may prove useful in estimating the amount of energy in similar configurations.

II. FORCE-FREE-FIELD CALCULATIONS

In a recent article, Yang, Sturrock, and Antiochos (1986) have proposed a new method for computing force-free magnetic-field configurations that they term the "magneto-frictional method" (see also Chudura and Schluter 1981; Craig and Sneyd 1986). This procedure has been applied to the present problem. The magnetic field is expressed in terms of Clebsch variables

$$\vec{B} = \nabla\alpha \times \nabla\beta\,, \tag{2.1}$$

where α and β are assumed to be of the form

$$\alpha = \alpha(x,y), \quad \beta = z - \gamma(x,y). \tag{2.2}$$

We see that

$$B_x = \frac{\partial\alpha}{\partial y}\,, \quad B_y = -\frac{\partial\alpha}{\partial x}\,, \quad B_z = -\frac{\partial\alpha}{\partial x}\frac{\partial\gamma}{\partial y} + \frac{\partial\alpha}{\partial y}\frac{\partial\gamma}{\partial x}\,. \tag{2.3}$$

Since α and β are each constant along a field line--because the divergence of the field must vanish--it is clear that the function $\gamma(x,y)$ shows how each field line is displaced in the z direction.

In this model, the plane $y = 0$ is taken to be the photosphere, and the z axis is the axis of the line dipole. Hence the normal component of the photospheric magnetic field is $B_y(x,0)$.

We consider two different distributions of flux in the photosphere. The first is given by

$$\alpha_1(x,0) = \exp(- x^2 / x_0^2) \tag{2.4}$$

so that

$$B_{y1}(x,0) = \frac{2x}{x_0^2} \exp(- x^2 / x_0^2) . \tag{2.5}$$

Figure 1 shows how $B_{y1}(x,0)$ varies with distance from the dipole axis for the adopted value $x_0 = 4$.

Klimchuk (1987) has recently pointed out that active region fields are not generally distributed in this way, however. Instead of gradually increasing in strength away from the dipole axis, the normal field component tends to commence abruptly at some finite distance from the axis. This results in a "weak field corridor" that separates the opposite polarity strong fields of the active region. Similarly, the normal field tends to end abruptly at the perimeters of active regions, rather than gradually falling to zero. We therefore consider a second, more realistic field distribution, also shown in Figure 1 and given by

$$\alpha_2(x,0) = \left(d + \frac{4}{\pi}\right)^{-1} \frac{x}{|x|} \begin{cases} d + \frac{4}{\pi} & |x| \le c \\ \frac{2}{\pi}\cos\left[(|x| - c)\frac{\pi}{2}\right] + d + \frac{2}{\pi} & c < |x| \le c+1 \\ -x + c + d + 1 + \frac{2}{\pi} & c+1 < |x| \le c+d+1 \\ \frac{2}{\pi}\cos\left[(|x| - c - d)\frac{\pi}{2}\right] + \frac{2}{\pi} & c+d+1 < |x| \le c+d+2 \\ 0 & |x| > c+d+2 \end{cases} \tag{2.6}$$

so that

$$B_{y2}(x,0) = \left(d + \frac{4}{\pi}\right)^{-1} \frac{x}{|x|} \begin{cases} 0 & |x| \le c \\ \sin\left[(|x| - c)\frac{\pi}{2}\right] & c < |x| \le c+1 \\ 1 & c+1 < |x| \le c+d+1 \\ \sin\left[(|x| - c - d)\frac{\pi}{2}\right] & c+d+1 < |x| \le c+d+2 \\ 0 & |x| > c+d+2 \end{cases} . \tag{2.7}$$

Here, c is the corridor half-width and d+2 is the size of the strong field region, or "plage." We choose c = 1 and d = 4. Units are arbitrary, but correspond to approximately 10^4 km on the Sun. The field has been normalized so that both distributions contain the same amount of positive and negative flux.

To study the effects of stress in the field, we assume there is a region of the photosphere within the band $|x| \le x_1$ that is subject to a shearing motion parallel to the z axis. There is no shearing motion outside that band. Our specific assumption is that

$$\gamma(x,0) = \left\{ \begin{array}{ll} Z_{max} \sin\left(\frac{\pi x}{x_1}\right) \left|\sin\left(\frac{\pi x}{x_1}\right)\right| & |x| \le x_1 \\ 0 & |x| > x_1 \end{array} \right\} . \qquad (2.8)$$

Hence Z_{max} is a measure of the relative shear of the two parts of the dipole. Figure 2 shows the shape of this shear function for the three cases $x_1 = 2$, 4, and 8. In two cases the shear is concentrated toward the central part of the dipole, and in the third it is more evenly distributed. For the case $x_1 = 2$, the shear occurs almost entirely within the weak field corridor of $B_{y2}(x,0)$, and we do not examine this uninteresting possibility.

To calculate a force-free field using the magneto-frictional method, one assumes photospheric boundary conditions such as those above and specifies an initial guess at the overlying coronal field. This field is then allowed to relax subject to the Lorentz forces and to a ficticious friction force which makes the relaxation well-behaved. At all times α and γ are held constant on the boundary.

In carrying out the calculations, it is necessary to introduce an artificial outer boundary within which the entire magnetic field is contained. The numerical "box" we have thus adopted has dimensions of 80 in the x-direction and 60 in the y-direction. (In fact, we use only half of this box since the $x = 0$ plane is a plane of symmetry.) At the outer boundary we impose the condition $\alpha = 0$, which is equivalent to assuming that the boundary is "superconducting." The boundary is sufficiently distant, however, that it has negligible effect on total field

energy. At the $x = 0$ plane we require only that α be symmetric and γ be antisymmetric, and we allow the field lines to slip.

The relaxation to a force-free state is performed on a finite-difference grid using an explicit, second-order differencing scheme. To adequately resolve the field with a manageable number of grid points we have adopted a nonuniform grid having cells of equal size in the region $0 < x < 10$, $0 < y < 10$, and cells of exponentially increasing size in the region beyond. The minimum and maximum cell dimensions are 0.5 and 2.3, respectively (except in the models with $x_l=2$, where the minimum dimension is 0.33).

The rate of relaxation is enhanced considerably by performing the calculation in three separate stages--first using a coarse grid and then mapping onto successive grids of increasingly finer resolution. The field so obtained is nearly force-free field within just a few hundred iterations. We nonetheless allow our models to run for at least 5000 iterations to achieve the highest degree of accuracy. At the end of the calculations the field and current are aligned to within a fraction of a degree, and the energy changes by only one part in 10^6 during each iteration.

In principle, the final equilibrium configuration may not be unique, since there can be other configurations--with more complicated topologies, perhaps including "magnetic islands"--that satisfy the same boundary conditions. We find, in practice, that our procedure selects the simplest, lowest energy state accessible to the field for the given boundary conditions. Unwanted topological complexities are eliminated by numerical dissipation inherent in the computations.

It is worth noting that the computer code used for the present study was developed independently of that used by Yang, Sturrock, and Antiochos (1986). As a check, we have repeated the calculations made by those authors and find that the earlier results are fully corroborated. This gives us confidence that both codes are working correctly. Most of the present calculations were performed on a Macintosh II work station.

III. NUMERICAL RESULTS

The results of two of our calculations are shown in Figure 3. Figure 3a shows the contours α = constant in the x-y plane for the normal field distribution $B_{y1}(x,0)$ in the case of no currents ($Z_{max} = 0$). Figure 3b shows the corresponding contours for the stressed case $x_1 = 4$, $Z_{max} = 10$. *These contours are the projections of field lines onto the x-y* plane, and therefore give the "end-on" view of field lines. Figure 3c gives the same contours in the y-z plane, showing the "side view" of the field lines. Figure 3d shows the contours in the x-z plane, representing the "top view" of the field lines.

We note that, as found earlier by Sturrock and Woodbury (1967), the effect of the shear displacement is to "inflate" the magnetic field configuration, since the development of the B_z component has the same effect as gas pressure. In this context, it is interesting to note that B_z = constant along each field line (see Appendix A).

Careful readers will see that, for the $\alpha = 0.4$ contour in Figure 3d, the endpoints are not the furthest removed points from the z-axis. This implies that B_z changes sign along the field line, in contradiction with the result of Appendix A. We can attribute this discrepancy to the finite

grid nature of our calculations. In general, finite-difference equations do not yield exactly the same solution as the continuous equations from which they are derived, and since Appendix A is based on the continuous equations, it applies only approximately to the model calculations.

In Figure 4, we give the total energy of the magnetic field as a function of shear for the five different configurations we have considered. Panels on the left side of the figure are for the normal field distribution $B_{y1}(x,0)$, and panels on the right side are for the normal field distribution $B_{y2}(x,0)$. The width of the shear zone, x_1, decreases from 8 in the top row, to 4 in the middle row, to 2 at the bottom. As expected, the energy is found to increase monotonically with shear. In each case the maximum displacement (Zmax = 16) produces a stressed field with roughly 3 times the energy of the corresponding potential field. There is an important difference between these curves and the corresponding curve for the case of cylindrical symmetry given in Wang, Sturrock, and Antiochos (1986). In the case of cylindrical symmetry, the total energy tends asymptotically to the (finite) energy of the open field. Such behavior is not possible in the present geometry, since the energy of the corresponding open-field configuration is infinite.

Low (1982), following Raadu (1971) and Low and Nakagawa (1975), has considered a sequence of solutions of the force-free equations, for fields of translational symmetry. Any sequence is defined by a "generating function," related to the functional form of the dependence of B_z upon α. Such a sequence is quite different from the sequences we consider, in which the shear displacement has a specified functional

dependence on the transverse variable x. Hence, it is not surprising that the evolution of a sequence in Low's model is quite different from the evolution of a sequence in our's. Whereas one of Low's sequences typically ends at a state of finite energy, our sequences do not terminate, and the energy becomes arbitrarily large.

An important difference between the present models and the earlier numerical models of Sturrock and Woodbury (1967) and Yang, Sturrock, and Antiochos (1986) is that there is, in the present models, an outer shell of magnetic flux that suffers little or no shearing displacement. These field lines therefore tend to restrain the tendency of the inner flux region to expand into an open configuration. As a result, the outer boundary has a much smaller effect on these calculations than it had in the previous cases.

We can estimate the effect of the outer boundary on the field energy by multiplying the mean value of energy density at the boundary ($B^2 / 8\pi$) by the volume of the computational box. This crudely represents the work that would be done by the field in expanding to infinity. The energy uncertainty obtained in this way reaches an extreme value of 4 % for the most severly sheared cases in which $x_1 = 8$ (and in which the outer shell of unsheared flux is smallest). The uncertainty is less than 1 % for most of the models, however, so we can be confident that we overestimate the energy by at most a few percent.

IV. EMPIRICAL MODEL FOR MAGNETIC ENERGY VARIATION

A single numerical calculation yields an exact answer to a single question, but an analytical solution shows how the quantity of interest depends on the parameters characterizing the problem. It would be very

convenient to have an understanding of the variation of the total magnetic energy as a function of shear and, for this reason, we have attempted to find a simple functional form that approximates the form of the curves shown in Figure 4.

If S is a normalized measure of the shear, such as Z / W, where Z is a measure of the shear and W is a measure of the width of the bipolar region, we expect that the total magnetic energy U can be expressed as

$$U = U_0 \, F(S) \ , \tag{4.1}$$

where U_0 is the total energy of the current-free field that corresponds to S = 0. Hence F(0) = 1. It is also clear that F must be an even function of S so that it is expressible as a function of S^2.

We now consider the asymptotic state of the magnetic field for very large values of S. As S tends to infinity, the magnetic field is driven more and more towards an open configuration. For some very large value of S, we expect that the field is substantially open as far as a radius $r \approx KS$, but remains substantially dipolar in form for $r > KS$. Hence for $r \leq KS$, $B \propto r^{-1}$, whereas for $r > KS$, $B \propto r^{-2}$.

One may therefore estimate the dominant contribution to the magnetic energy by calculating the energy of the magnetic field as far as r = KS:

$$U(S) \propto \int_{r_0}^{KS} \pi \, r \, dr \cdot \frac{1}{8\pi} \frac{1}{r^2} \ . \tag{4.2}$$

Hence we expect that, for large values of S,

$$U(S) \propto \ln S \ . \tag{4.3}$$

A simple function that has this asymptotic behavior, is an even function of S, and reduces to U_0 for S = 0, is

$$U(S) = U_0 \ [\ 1 + a \ln(1 + b\, S^2)\ ] \ . \tag{4.4}$$

In Table 1, we give the calculated values of U / U_0 for the normal field distribution $B_{y1}(x,0)$ with $x_1 = 4$ and Z_{max} in the range 0 to 16. Adopting $S = Z_{max} / x_0 = Z_{max} / 4$ (so that $2Z_{max}$ is the maximum displacement of any field line, and $2x_0$ is a measure of the total width of the field), the values of S are as shown in the table. We have made a least-squares fit to these data and found that the best fit is obtained for $a = 0.8156$, $b = 0.8318$. With these values, the formula (4.4) yields the estimates of U / U_0 shown in the third column of Table 1. We see that the average discrepancy between the estimated and actual values of the energy is only 0.4 %. This good agreement is evident in Figure 4 (middle left panel) where the fit to the model data is shown as a solid curve.

In Table 2 we list the values of a and b determined for each of the five configurations we have modeled. As can be seen from the average discrepancies provided in column 5 and from the close agreement in Figure 4, the quality of the fits is exceptional in each case. It would seem from this result that the energy of a line dipole can always be expressed as a simple function of shear in terms of the two parameters a and b.

The pair (a, b) is unique to each configuration, however, and it would be useful to have a single function with universal parameters a*and b* that is able to describe all situations. The values of a and b given in Table 2 are not too widely varied, but is easy to imagine other configurations for which at least one of the parameters would be well outside the range in the table. For example, if the shear were localized in a region where the flux is weak, say in the extreme outer region of distribution $B_{y1}(x,0)$, then the energy of the field would be only a very weak function of S. Clearly, therefore, a general formula relating energy to shear must somehow weight the shear according to the amount of flux that is affected.

As a first attempt, we replotted the energy data using the abscissa $S_1 = Z_1 / W_1$, where

$$Z_1 = \int_0^\infty \gamma(x,0)\ [B_y(x,0)]^2\ dx\ , \tag{4.5}$$

and

$$W_1 = \int_0^\infty x\ [B_y(x,0)]^2\ dx\ . \tag{4.6}$$

Figure 5 shows the resulting plot for all five configurations combined. It is obvious that this particular definition of shear does not produce a good energy-shear correlation.

We note that, for a given amount of shearing displacement (Δz), the field is more highly distorted near the dipole axis than away from it. That is, the projection of a field line onto the photosphere makes a smaller angle with the dipole axis for field lines that originate closer to

the axis. Since greater distortion usually implies greater energy, it is reasonable to suppose that a definition of shear that takes this into account might produce a tighter energy-shear correlation. We have therefore replotted the data using the following two abscissas:

$$S_2 = \frac{\int_0^\infty \frac{\gamma(x,0)}{x} [B_y(x,0)]^2 \, dx}{\int_0^\infty [B_y(x,0)]^2 \, dx} \tag{4.7}$$

and

$$S_3 = \left[\frac{\int_0^\infty \left[\frac{\gamma(x,0)}{x}\right]^2 [B_y(x,0)]^2 \, dx}{\int_0^\infty [B_y(x,0)]^2 \, dx} \right]^{1/2} . \tag{4.8}$$

We find that the energy-shear correlation using S_2 is improved, but that the correlation using S_3 is very satisfactory. This is shown in Figures 6 and 7. A least-squares fit of equation (4.4) to the data, substituting S_3 for S, yields the values $a = 0.7684$ and $b = 0.5530$. The average discrepancy between the data and fit is 3.5 %.

It is interesting also to note from equation (4.4) that the force opposing the shear varies with S (or S_3) as:

$$F \equiv \left|\frac{dU}{dS}\right| = \frac{2abU_0}{1 + bS^2} , \tag{4.9}$$

so that it varies linearly with S for small values of S and inversely with S for large values of S. The maximum value of F is $ab^{1/2}U_0$ at $S = b^{-1/2}$. Since the normal field B_y is being held constant at the photosphere, the above variation in F must be attributed to a progressive change in the value B_z, the component of field in the direction of shear: B_z first increases and then decreases with S.

V. DISCUSSION

We have seen from Section III that relative shearing motion of the two sides of a line dipole leads to "inflation" of the magnetic-field pattern and to a progressive increase in the stored magnetic energy. For such a model, the magnetic energy can, in principle, become arbitrarily large. Hence the free energy of a stressed magnetic field in an active region may in fact be considerably larger than the energy of the corresponding potential field. In this respect, the linear dipole configuration differs significantly from cylindrically symmetric models, such as the one considered by Wang, Sturrock, and Antiochos (1986).

We have also found that a simple analytical model provides a good fit to *all* of our calculated fields. Combining equations (4.4) and (4.8) this model can be represented by the formula

$$U(Z_{max}) = U_0 \, [\, 1 + a^* \ln(1 + \hat{b}\, Z_{max}^2) \,] \, , \qquad (6.1)$$

where

$$\hat{b} = b^* \frac{\int_0^\infty \left[\frac{f(x,0)}{x}\right]^2 [B_y(x,0)]^2 \, dx}{\int_0^\infty [B_y(x,0)]^2 \, dx}, \tag{6.2}$$

$$f(x,0) = \frac{\gamma(x,0)}{Z_{max}}, \tag{6.3}$$

and

$$a^* = 0.7684, \qquad b^* = 0.5530.$$

Note that a^* is identical to a in equation (4.4). This is consistent with the small range of a values in Table 2.

The fact that the magnetic energy, as a function of shear, may be expressed in a simple functional form suggests that it may be possible to find a simple approximate representation of the magnetic field itself.

If formula (6.1) is indeed general, as our results would suggest, then the total energy contained in *any* line dipole field can be easily determined as a function of the shear amplitude, Z_{max}. One needs only specify the photospheric quantities $B_y(x,0)$ and $f(x,0)$--the normal field distribution and the form of the shearing displacement. (The energy of the potential field, U_0, is given uniquely by $B_y(x,0)$.)

This formula is useful for studying which types of photospheric conditions give rise to the greatest free energy in the corona. Ultimately, this energy may be used to power solar flares, coronal mass ejections, etc. We see from formula (6.2) that the magnetic energy is relatively more enhanced if the shearing displacement occurs: (1) where the

normal field is strongest; (2) in the inner region of the dipole, close to the axis; or (3) over a large fraction of the dipole area. These situations are of course not mutually exclusive.

We have seen that wholly different boundary conditions can produce very similar results. In our computed models the energy increases obtained with $x_1 = 2$ and $x_1 = 8$ are comparable, even though $x_1 = 2$ optimizes the second factor listed above while $x_1 = 8$ optimizes the third. In general, the relative importance of these various factors will depend on the details of the flux distribution in question. It is mostly a coincidence that the b values in Table 2 fall within a fairly small range of each other.

One attractive feature of our formula is that all of the quantities can, *in principle*, be measured. The normal component of field in the photosphere is routinely and fairly accurately measured by present-day longitudinal magnetographs. The form of the shear displacement is not so easily determined, on the other hand. Vector magnetographs are used for this purpose, but the observations are at this time both difficult to make and difficult to interpret (e.g., Skumanich and Lites 1987; Ronan, Mickey, and Orrall 1987). Perhaps the situation will improve with further developements in theory and with the new generation of instruments planned by HAO and the University of Hawaii, among others.

One could infer the form of the shear from features observed in H-alpha and in X-rays. The usefulness of H-alpha observations is limited, however, in that dark fibrils and filaments are seen only in the weak field corridors at the centers of active regions and in the surrounding weak field areas (Klimchuk 1987). X-ray images would provide valuable

information on the shear in the more important strong field regions, but our next opportunity for systematic observations will have to await the launch of Solar-A in 1991.

And finally, we end on a cautionary note. Our study has thus far been two-dimensional, yet active regions on the Sun, even those that resemble line dipoles, are not of infinite extent. To study more realistic configurations it will be necessary to use three-dimensional modelling, which is something we plan for the near future.

This work was supported in part by Office of Naval Research Contract N00014-85-K-0111, by NASA Grant NGL 05-020-272, and as part of the Solar-A collaboration under NASA Contract NAS8-37334 with Lockheed Palo Alto Research Laboratories.

APPENDIX A

Demonstration that B_z = const. along a field line.

We see from equation (2.3) that B may be expressed as

$$\vec{B} = \left(\frac{\partial \alpha}{\partial y}, -\frac{\partial \alpha}{\partial x}, B_z \right) . \tag{A.1}$$

Hence the current density $\vec{j}$ may be expressed as

$$\vec{j} = \frac{1}{4\pi} \left(\frac{\partial B_z}{\partial y}, -\frac{\partial B_z}{\partial x}, -\frac{\partial^2 \alpha}{\partial x^2} - \frac{\partial^2 \alpha}{\partial y^2} \right) . \tag{A.2}$$

The Lorentz force is zero for a force-free field, so the expression for the *z*-component of this force leads to the relation

$$\frac{\partial B_z}{\partial x} \frac{\partial \alpha}{\partial y} - \frac{\partial B_z}{\partial y} \frac{\partial \alpha}{\partial x} = 0 . \tag{A.3}$$

This shows that the projections of ∇B_z and $\nabla \alpha$ in the x-y plane are parallel. However, B_z and α are independent of z, so ∇B_z is parallel to $\nabla \alpha$. We see from equation (2.1) that $B \cdot \nabla \alpha = 0$. Hence $B \cdot \nabla B_z = 0$, showing that B_z = const. along a field line.

TABLE 1

Comparison of Computed Energy (U / U_0) and Best Fit (U_f / U_0)

For the Case $B_{y1}(x,0)$, $x_1 = 4$

S	U / U_0	U_f / U_0
0.0	1.000	1.000
0.5	1.171	1.154
1.0	1.507	1.494
1.5	1.859	1.860
2.0	2.185	2.195
2.5	2.477	2.488
3.0	2.737	2.744
3.5	2.970	2.970
4.0	3.180	3.170

TABLE 2

Energy vs. Shear Fit Parameters

Normal Field Distribution	x_1	a	b	Average Discrepancy
$B_{y1}(x,0)$	8	0.7437	0.4755	0.44 %
$B_{y1}(x,0)$	4	0.8156	0.8318	0.43 %
$B_{y1}(x,0)$	2	0.6354	0.6234	0.82 %
$B_{y2}(x,0)$	8	0.7752	0.4544	0.47 %
$B_{y2}(x,0)$	4	0.7489	0.6071	0.49 %

REFERENCES

Athay, R. G., Klimchuk, J. A., Jones, H. P., and Zirin, H. 1986, Ap. J., **303**, 884.

Chodura, R., and Schluter, A. 1981, Journal of Comp. Physics., **41**, 68.

Craig, I. J. D., and Sneyd, A. D. 1986, Ap. J., **311**, 451.

Hagyard, M. J., ed. 1985, Measurements of Solar Vector Magnetic Fields (NASA Conference Pub. 2374).

Klimchuk, J. A. 1987, Ap. J., **323**, 368.

Low, B. C. 1982, Reviews of Geophys. and Space Phys., **20**, 145.

Low, B. C., and Nakagawa, Y. 1975, Ap. J., **199**, 237.

Raadu, M. A. 1971, Astrophys. Space Sci., **14**, 464.

Ronan, R. S., Mickey, D. L., and Orrall, F. Q. 1987, Solar Phys., submitted.

Simon, G. W., et al. 1988, Ap. J. (in press).

Skumanich, A., and Lites, B. W. 1987, Ap. J., **322**, 473.

Sturrock, P. A., and Woodbury, E. T. 1967, in Plasma Astrophysics, ed. P. A. Sturrock (New York: Academic Press), p. 155.

Svestka, Z. 1976, Solar Flares (Dordrecht-Holland: Reidel).

Webb, D. F. and Zirin, H. 1980, Solar Phys., **69**, 99.

Yang, W.-H., Sturrock, P. A., and Antiochos, S. K. 1986, Ap. J., **309**, 383.

FIGURE CAPTIONS

Figure 1.--Assumed distributions of the photospheric normal field as a function of distance from the dipole axis. The distributions are anti-symmetric about the dipole axis, so that positive B_y on one side of the dipole corresponds to negative B_y on the other side.

Figure 2.--Assumed distributions of photospheric shear as a function of distance from the dipole axis. The shear is anti-symmetric about the dipole axis, so that on one side of the dipole the footpoints are displaced in the positive z-direction and on the other side of the dipole they are displaced in the negative z-direction.

Figure 3.--Various views of the field lines, labeled by the value of α, for two different force-free field models having the normal field distribution $B_{y1}(x,0)$ and shear function parameter $x_1 = 4$: (a) projections of field lines on the x-y plane, giving the "end-on" view, for the current-free case $Z_{max} = 0$; (b) the same as (a), but for the stressed case $Z_{max} = 10$; (c) projections on the y-z plane, giving the "side-on" view, for the case $Z_{max} = 10$; and (d) projections on the x-z plane, giving the "top" view, for the case $Z_{max} = 10$.

Figure 4.--Energy versus shear plots for five different magnetic configurations distinguished by the normal field distribution and shear function parameter x_1. The ordinate is the normalized energy U / U_0, where U_0 is the energy of the potential field, and the abscissa is the

normalized shear $S = Z_{max} / 4$. Solid dots are from the model calculations and curves are from least-squares fits of equation (4.4).

Figure 5.--Plot of energy versus shear (S_1) for all five magnetic configurations combined. The abscissa S_1 is defined by equations (4.5) and (4.6). Open symbols are for normal field distribution $B_{y1}(x,0)$ and solid symbols are for distribution $B_{y2}(x,0)$. Triangles, circles, and squares represent the cases $x_1 = 8$, 4, and 2, respectively.

Figure 6.--Plot of energy versus shear (S_2) for all five magnetic configurations combined. The abscissa S_2 is defined by equation (4.7). Open symbols are for normal field distribution $B_{y1}(x,0)$ and solid symbols are for distribution $B_{y2}(x,0)$. Triangles, circles, and squares represent the cases $x_1 = 8$, 4, and 2, respectively.

Figure 7.--Plot of energy versus shear (S_3) for all five magnetic configurations combined. The abscissa S_3 is defined by equation (4.8). Open symbols are for normal field distribution $B_{y1}(x,0)$ and solid symbols are for distribution $B_{y2}(x,0)$. Triangles, circles, and squares represent the cases $x_1 = 8$, 4, and 2, respectively. The curve is a least-squares of equation (6.1).

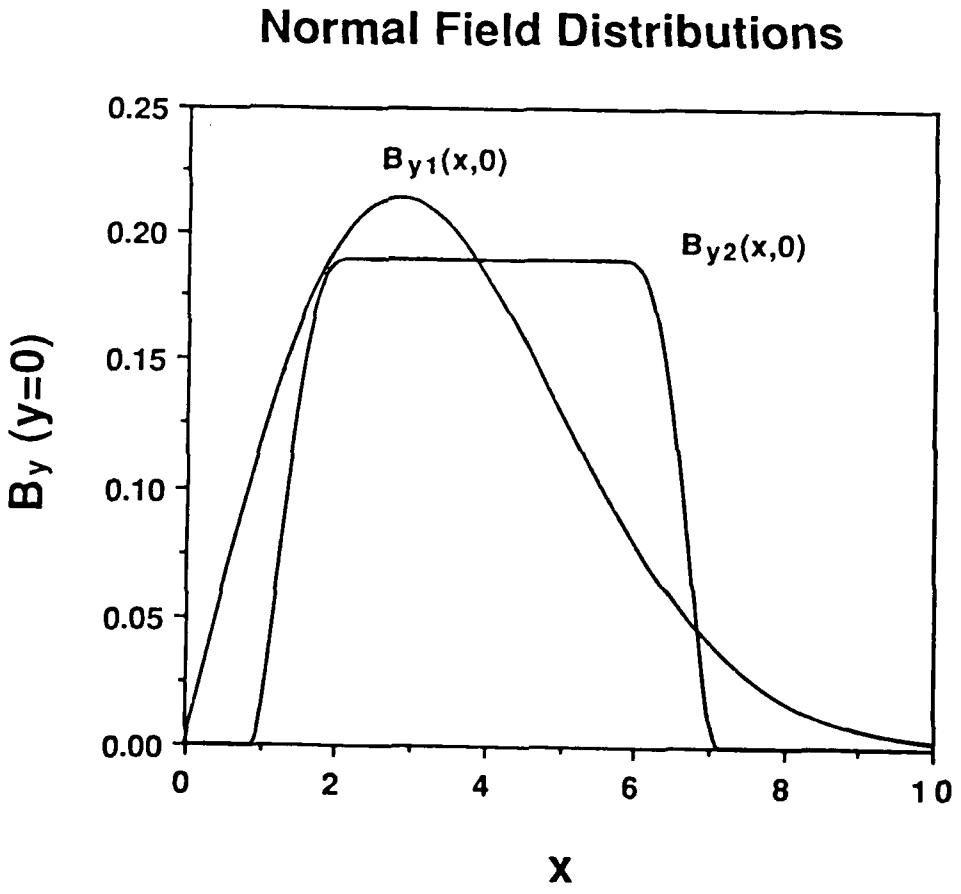
Normal Field Distributions
0.25
0.20
0.15
0.10
0.05
0.00
By (y=0)
By1(x,0)
By2(x,0)
0
2
4
6
8
10
X

Figure 1.

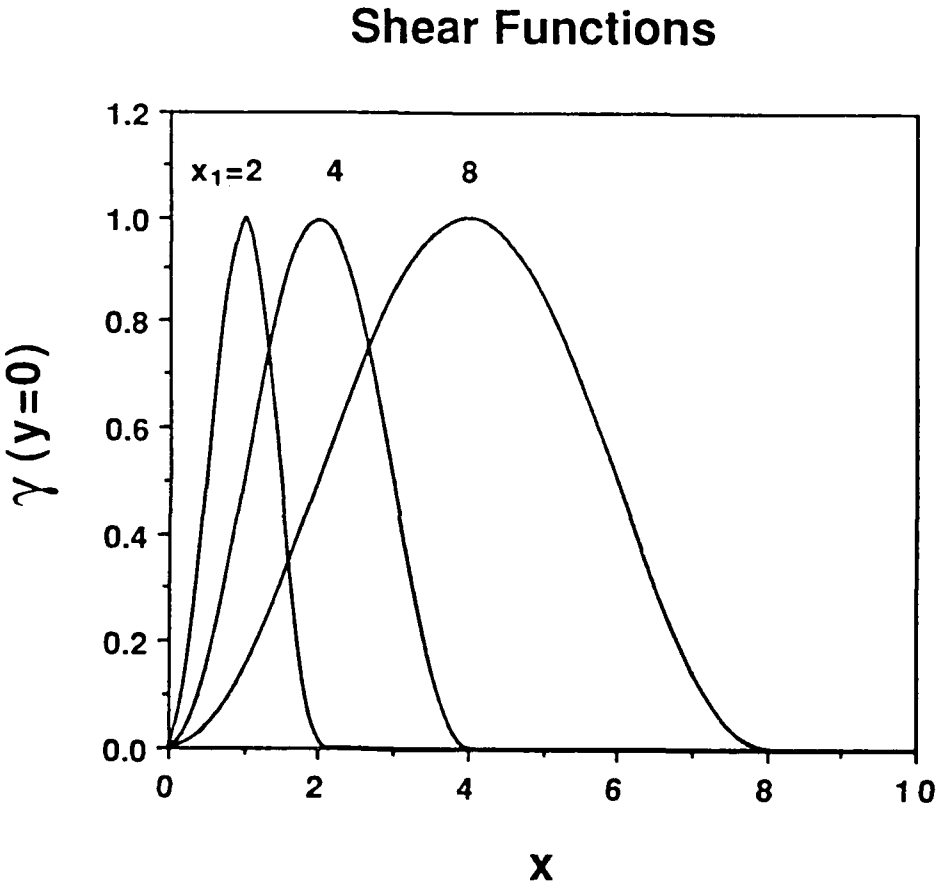

Figure 2.

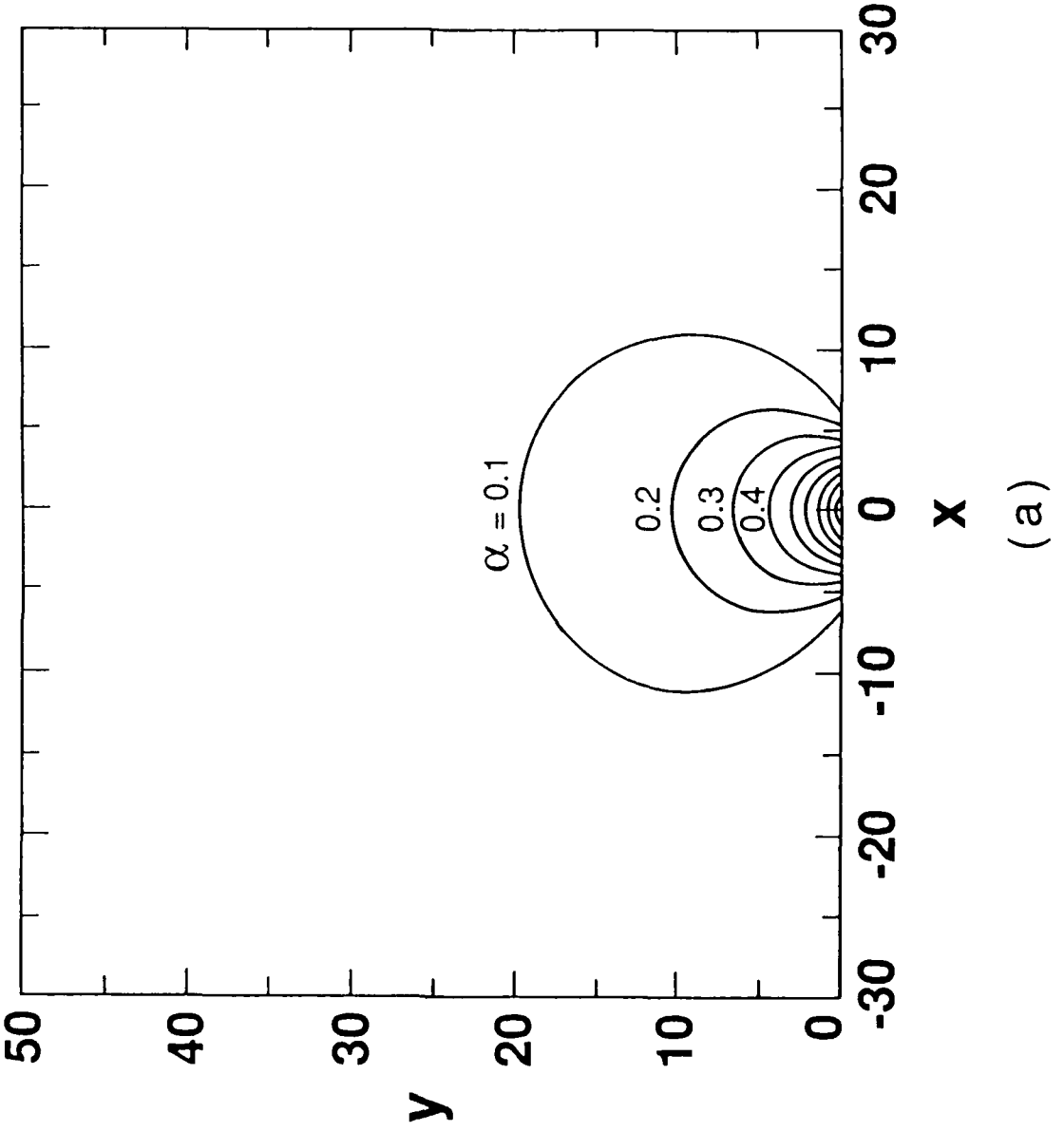

Figure 3.

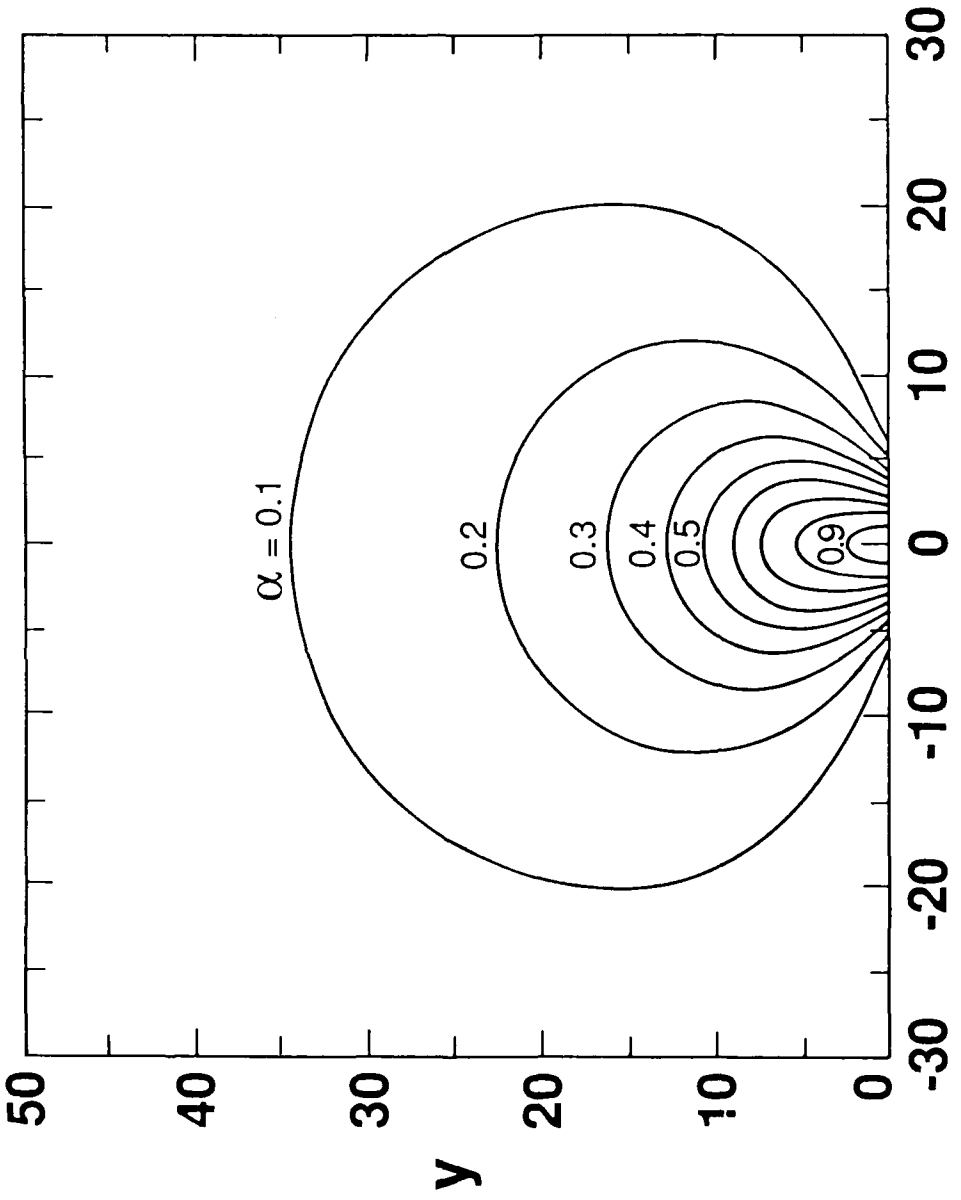

Figure 3.

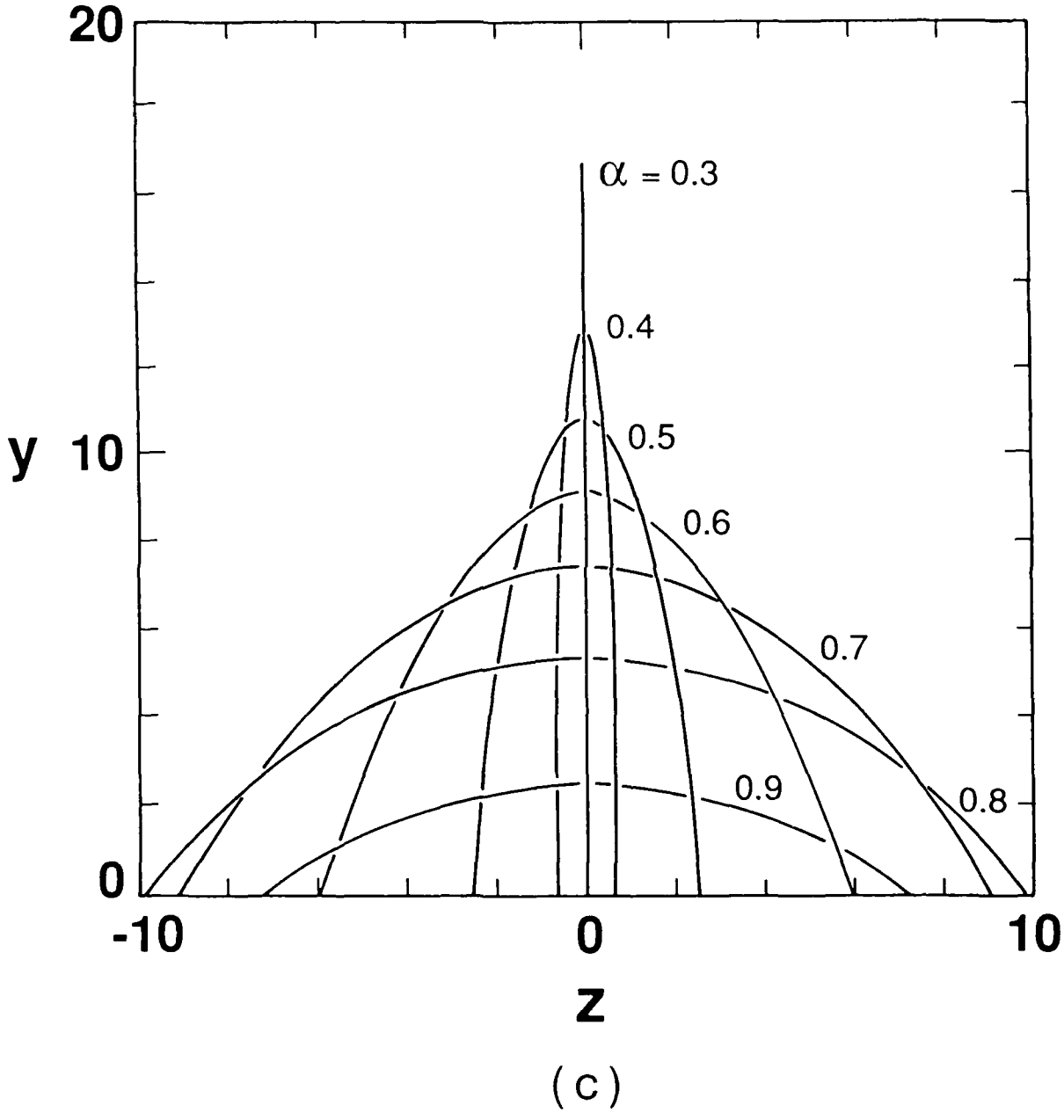

Figure 3.

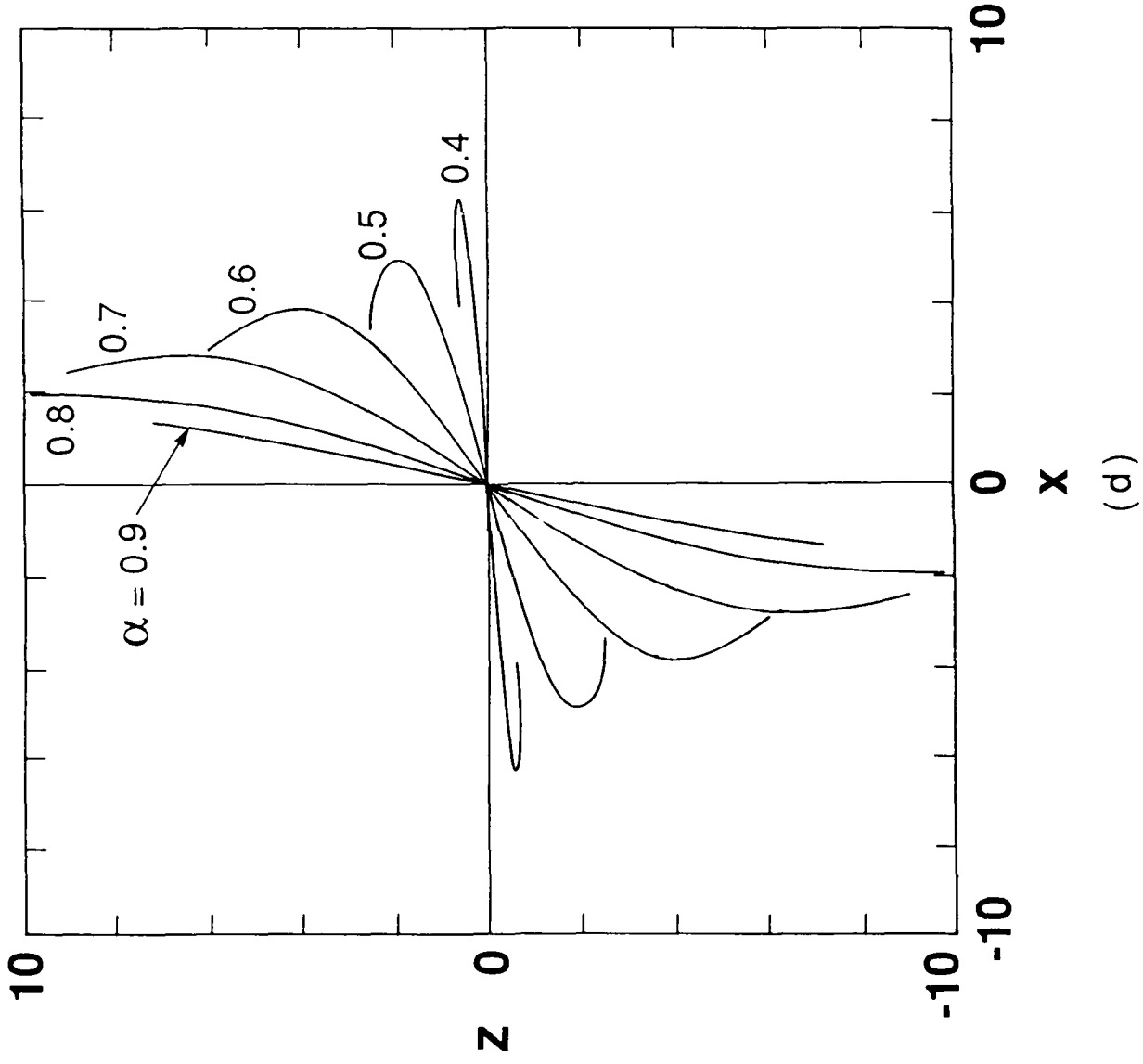

Figure 3.

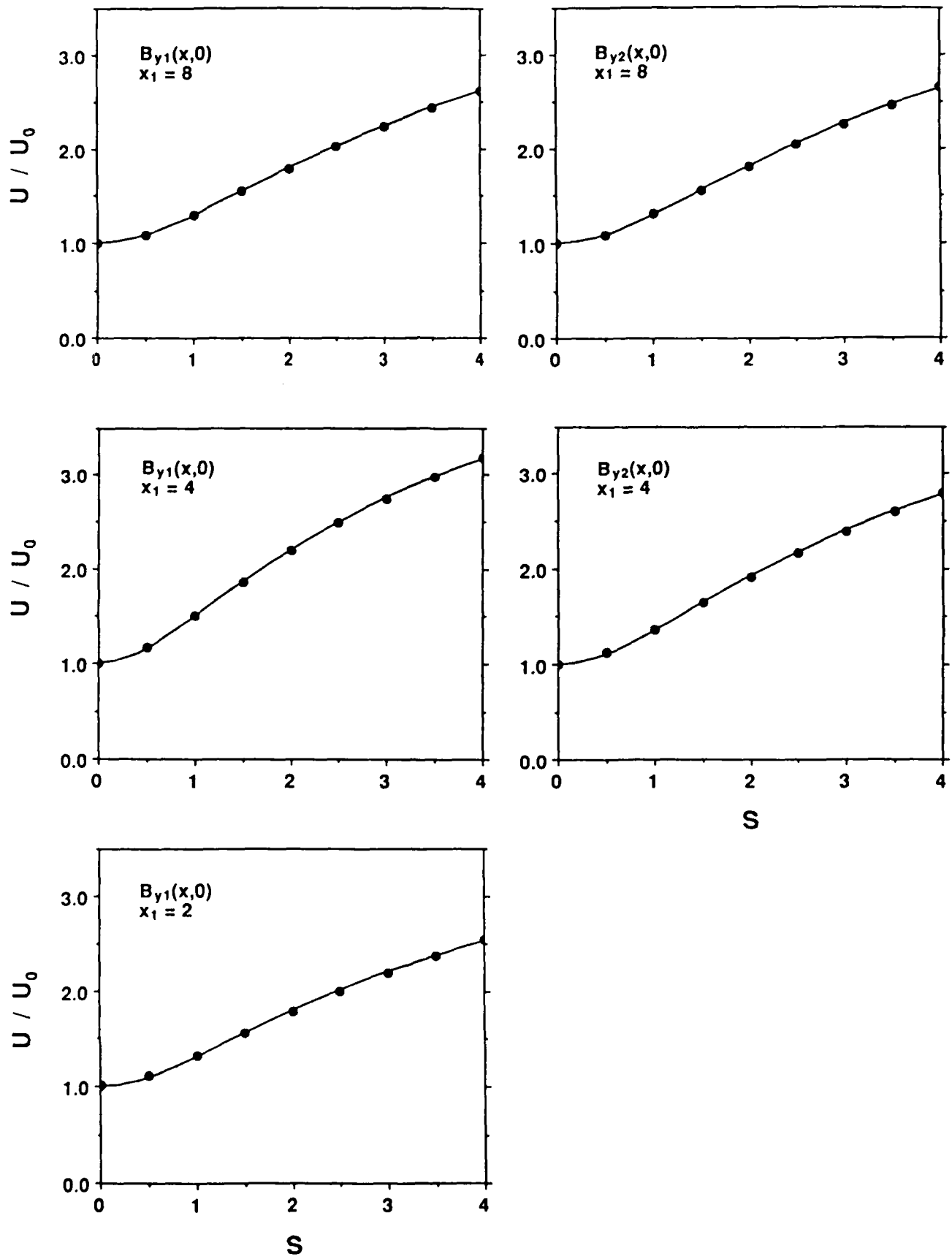
$B_{y1}(x,0)$
$x_1 = 8$
$B_{y2}(x,0)$
$x_1 = 8$
$B_{y1}(x,0)$
$x_1 = 4$
$B_{y2}(x,0)$
$x_1 = 4$
$B_{y1}(x,0)$
$x_1 = 2$
U / U0
S
0.0
1.0
2.0
3.0
0
1
2
3
4

Figure 4.

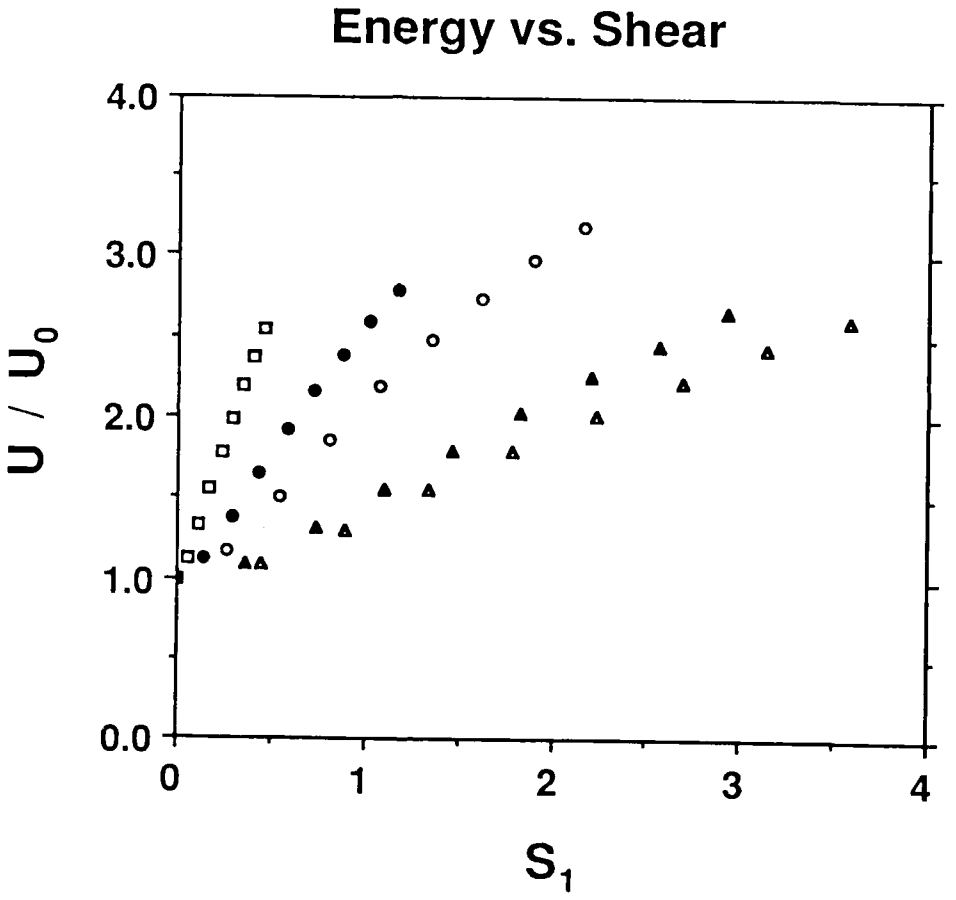

Figure 5.

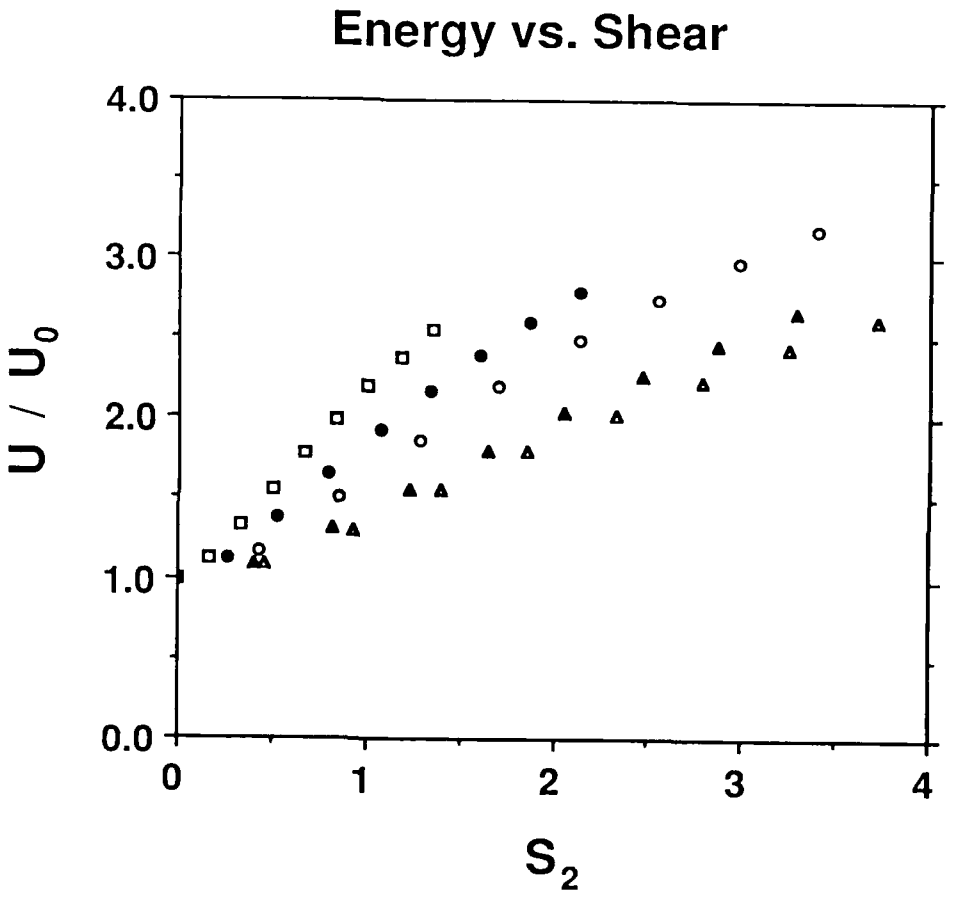

Figure 6.

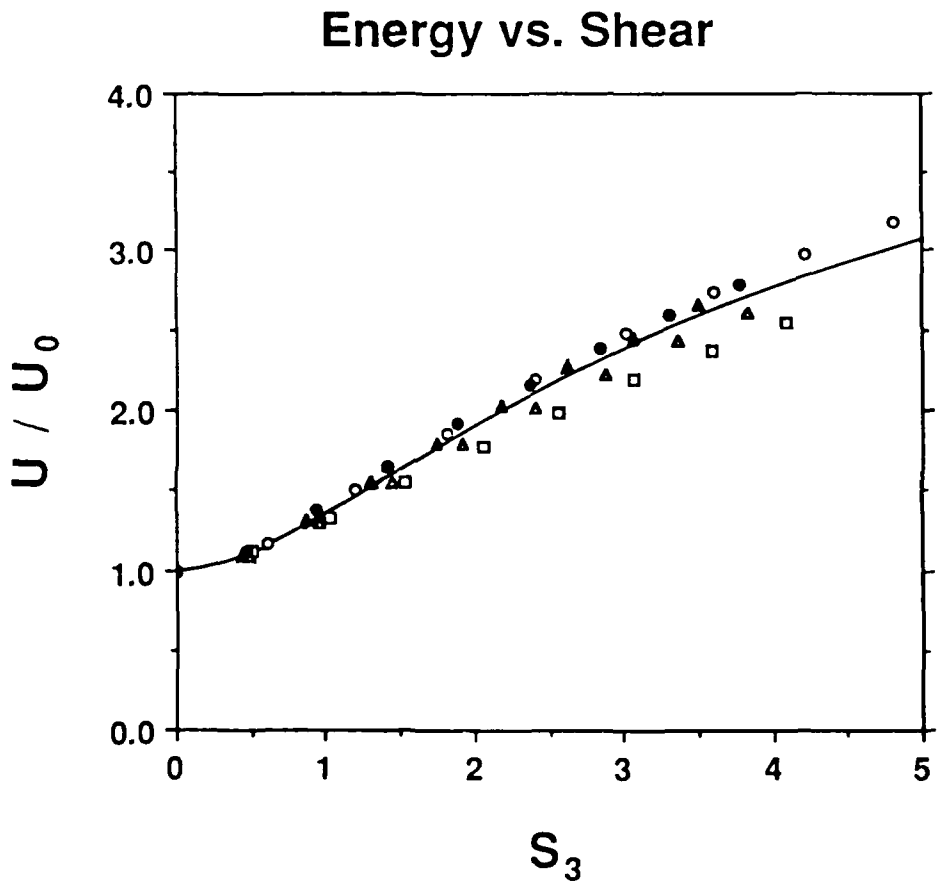

Figure 7.

POSTAL ADDRESSES

JAMES A. KLIMCHUK: Center for Space Science and Astrophysics, Stanford University, ERL 300, Stanford, CA 94305

PETER A. STURROCK: Center for Space Science and Astrophysics, Stanford University, ERL 306, Stanford, CA 94305

WEI-HONG YANG: Center for Atmospheric and Space Sciences, Utah State University, Logan, UT 84322-4405

END
DATED
FILM
8-88
DTIC